1-12-2017

Exploration of Thin Film Polymers for Phosphor Thermometry

Pratikshya Parajuli

EXPLORATION OF THIN FILM POLYMERS FOR PHOSPHOR THERMOMETRY

by

Pratikshya Parajuli

A Thesis

Submitted in Partial Fulfillment of the

Requirements for the Degree of

Master of Science

Major: Physics

The University of Memphis

December, 2016

ACKNOWLEDGEMENT

During my short stint at University of Memphis and the preparation of this thesis, I met many people without whose help this work wouldn't have been possible. Firstly, I would like to express my sincere and special gratitude to my adviser Prof. Firouzeh Sabri for her guidance, unfailing help and continuous encouragement in this project. Despite my ignorance, she encouraged me to work in this field, and provided me support as a guardian at every point of this research.

I would also like to thank Dr. Allison who has been an important part of my research, Dr. Alam who was there whenever I needed him. Also, am thankful to Dr. Mishra for allowing me to work in his lab when I needed. I am also grateful to all my friends and seniors who helped me in completing this work.

Finally, I would like to dedicate this thesis to my parents for their love, inspiration and supporting me in my every success. Their encouragement and assistance was of great importance. I'll be indebted to them throughout my life.

List of Figures

Contents

Abstract

Phosphor thermometry has been investigated in recent years as means to explore instantaneous remote thermometry. Many different types of thermographic powders exist. In most cases work has been performed on these materials while in a fine powder form. There are significant challenges when working with fine powders (nm-μm particle size) and these challenges have limited the range of characterizations and potential applications of these materials. Among the different types of thermographic phosphors La_2O_2S:Eu is one of the most sensitive types that is currently available. Lanthanum oxysulfide doped with Eu has been reported to have a sensitivity of 0.01 °C with a wide temperature range of response-cryogenics to 1500 °C. In this work two types of La_2O_2S:Eu (0.1 % and 1.0 % Eu concentration) have been fully characterized at cryogenic temperatures and at elevated temperatures while embedded in an elastomeric sleeve. The flexible optically transparent elastomer Sylgard 184 was chosen as the encapsulant for this study. Samples with increasing levels of La_2O_2S:Eu powder (from 1 wt % to 25 wt%) were prepared and studied. Both single layer (single concentration) and multilayer (concentration gradient) sample types were prepared using spin-coating techniques and fully characterized. The effect of the La_2O_2S:Eu particles on the thermal, mechanical, and luminescence behavior of the composite materials was fully investigated and reported here. While the percentage of the Eu (0.1% versus 1.0%) did not have a detectable effect on the emission characteristics of the composites, it did indeed affect the thermal and mechanical properties of the composites. SEM investigation suggests that the differences in the granular structure of

the two powders has influenced the properties of the composite polymers prepared in this study. Furthermore, the emission behavior of the La_2O_2S:Eu+Sylgard184 composites showed a strong non-linear temperature dependence in the range of -40 °C to 75 °C and little dependence on the powder concentration level.

Chapter 1

Introduction

1.1 Phosphor thermometry

Phosphor-based thermography is a low-cost, portable, rapid, and noninvasive thermal detection technique with a high degree of precision where the luminescence properties (decay time and amplitude) reflect the temperature of the material. A variety of industries have taken advantage of phosphor thermometry and recently they have been investigated for biomedical applications as well the method makes use of phosphor materials identical or similar to many that are manufactured for lighting, display, scintillation, or medical X-ray applications. Typically, a phosphor is selected for the temperature range of the application and painted or otherwise coated onto the surface whose temperature is of interest. Luminescence is stimulated either directly or with the aid of lenses and/or optical fibers. Any of several emission characteristics such as lifetime or ratio of different spectral emission bands can indicate temperature [1]. An advantage of phosphor-based thermometry is that temperature-dependent luminescence can be measured from a distance and even through intervening scattering or partially absorbing media [2]. Elastomers from the family of polydimethylsiloxane (PDMS) are flexible and inert polymers with tunable chemical, physical, and electrical properties used in some cases for biomedical and in vivo applications [3].

1.2 Challenges associated with working with phosphor powders

The visible-light-generating components of emissive, full color, flat panel displays are called phosphors [4]. When it comes to phosphor thermometry measurements, the phosphor compound must be sprayed directly onto the surface of interest as a thin uniform film or with a mixture of an adhesive agent [5][6]. This can create surface imperfections, on the surface that is being coated and sin some cases applying a thin film coating can be extremely difficult. Finally, the phosphors that are used in this manner are no longer reusable.

1.3 Existing methods of temperature measurement and their limitations

Different methods for the remote temperature measurements are there. For example, electronic thermometers, infrared pyrometers, liquid crystals etc. however, they all have some limitations to their performance. Thermocouple, although work very nicely when fine, fail to prove useful to relatively benign flames [8]. Pyrometers, on the other hand, work by receiving an infrared energy from the target. However, they receive the energy from its surroundings when they receive energy from the target and may lead to pseudo information. Accurate information regarding temperature measurement is provided by the electronic thermometers which include thermocouples, digital thermometers, thermistors and etc. The disadvantages come when they provide little immunity to electromagnetic interference. The heating up of the metallic leads due to the electromagnetic waves may lead to the inaccurate measurements [9]. Liquid crystal gives the temperature information

from a large surface area resulting in the temperature drift, so anyone will be in dilemma regarding which data to use.

1.4 Advantages of composite polymers

In an attempt to create a non-destructive means to assess surface temperature, papers published before [1][7] have demonstrated the feasibility of Thermographic Phosphor thermometry with the phosphor particles encapsulated within an elastomeric polymer casing with no adverse effects on the emission characteristics and temperature response of the thermographic phosphors used [10]. The properties of the combined material can be tuned to deliver the sensitivity of choice by controlling the dopant concentration, among other things [11].

1.5 Polymer encapsulated thermographic phosphor temperature sensors

Thermal measurements involving thermographic phosphors, whether in the form of powder, crystal, or glass, continue to be of interest for a wide range of applications and temperature ranges [12]. A laser of definite wavelength is incident on the sample and the emission is observered, from where the decay time is calculated and the temperature of the sample is known. Previous work with thick films (prepared using drop-cast methods) where the phosphor powder is encapsulated in a polymeric matrix demonstrated that for the two phosphor types tested so far, the luminescence behaves the same way as the neat powder [1][13]. This suggests that chemical reaction between the polymer matrix and the phosphor powder is either negligible or, nonexistent. Earlier work published by authors has demonstrated the applicability of polymer composites loaded with phosphor for biomedical applications uti-

lizing optical, and X-Ray excitation mechanisms [3][14]. More recently, it was demonstrated that spin-coating techniques can be used to create thin flexible phosphor-doped films that are geometrically conformable, without detrimental effect to the decay characteristics of the thermographic phosphors used for the study [10].

The present account involves using spin-coating techniques to create multilayered structures with a gradient concentration of the phosphor powder and its luminescence thoroughly characterized between -45°C and 70°C, in a low humidity environment. Thin multilayer assemblies offer unique features that can (1) address the possible interplay of scattering and absorption, (2) establish signal levels for various thicknesses and concentrations, and, (3) develop a heat flux sensor. Here, the author presents the thermal, mechanical, and luminescence properties of multilayer, stacked, flexible thermographic phosphor temperature sensors.

1.6 Thesis Outline

In Chapter 2 the concepts and the mechanisms behind the luminescence, thermal conductivity and tensile test are shown by explaining the physics behind them. Also, information about phosphor thermometry and modeling related to thermal conductivity are presented. Methods and the materials used to follow the methods for the preparation of the required samples are explained in Chapter 3. Tree diagram has been shown to give a clear idea regarding the types of samples prepared along with their picture. Results produced after the different characterization when done with the samples are discussed in Chapter 4 while Chapter 5 concludes the result giving a brief description about the results. All the work that can be done with the future following the same technique applied to this research are explained in Chapter 6.

Chapter 2

Theory

2.1 Phosphor Thermometry

There are many ways to measure the temperature of any substance. But every technique has its own limitations. They can't be used everywhere.
For example, thermocouple can be used to measure the temperature. There are two wires from two different metals. A voltage is then produced from the junction between the two voltages which is proportional to the temperature of a surface in direct contact with the device. Thermocouples can accurately measure temperatures up to approximately 2500°C. However, their performance drops when exposed to oxidizing or reducing environments, such as in gas turbine engines. Also, non-stationary surfaces, such as turbine blades or pistons cannot be measured because thermocouples require direct physical contact with a surface. In the meantime, even the fluid dynamics of a given system can be spoiled.

Phosphor thermometry is a non-contact technique which uses optical signals to measure temperature remotely. However, this technique is not vulnerable to the issues of pyrometers, thermocouples, thermal paints, and many other thermal sensors. Phosphors are composed of a ceramic lattice doped with a small amount of luminescent ions which emit visible, infrared, or UV radiation upon excitation from an external energy source. The intensity, wavelength, or lifetime (duration of light) of the visible emission is used to determine the temperature of a surface. Unlike many other thermocouples and thermal paints, phosphors are composed of inorganic and ceramic materials

which means that phosphors are resistant to oxidation in high-temperature environments and are non-reactive with harsh chemicals.

If the matter is concerned with the measurement of temperature, phosphor thermometry has several major advantages over standard temperature measurement methods. Response of the phosphor does not depend on the surface properties, has the performance capacity from cryogenic system up to 2000K. Calibrated thermographic phosphors (TGP) do not drift over time. Very useful in measurement system with fast time dependency as TGPs have responsive time of microseconds [16].

2.1.1 Thermographic Phosphors

Phosphors are usually white in appearance and exhibit luminescence when excited by an external source of certain wavelength. Recently, they have wide range of applications from cathode ray tubes, plasma displays, light bulbs and x-ray conversion screens. The history of the phosphor goes back all the way to 1940s when the word phosphor came for the first time. After that, many researchers are working on it and have given their contribution in making phosphor [17].

TGP thermometry has many advantages over the conventional temperature sensors. TGPs can work over a wide range of temperature, i.e. cryogenic to 1800°C, remotely accessible, accuracy up to 0.05°C for some compounds, very economical, easily transportable, reusable, easy to store, and high versatility [10].

Phosphors are designed in many ways and the one that have been specifically designed for measuring temperature remotely are called thermographic phosphors. These materials consist of an oxide matrix and are doped with a rare-earth (RE) or transition metal ion [18]. After exciting the phosphor, the emitted luminescence can be observed in the UV, visible, or even in the

infrared region. Here, the luminescence is concentrated in the visible region. The emitted luminescence differs with the change in temperature [19] and this dependency has been used here to observe the various responses that change with temperature and make a sensor out of the phosphor (La_2O_2S:Eu).

2.1.2 Measurement Method

Since, phosphor emits energy as heat or lattice vibrations caused by the higher temperatures, they can be used as a thermal sensor. The change in the surface temperature highly affect the photo luminescent properties such as the luminescence wavelength, intensity, or lifetime. Surface temperature measurements are determined by evaluating experimental luminescent data against calibration data, which contain the temperature-dependence of a particular luminescent property. There are different ways to obtain the surface temperature such as evaluating the emission wavelength, intensity, or the lifetime (duration of the emission). In this work, we will focus on temperature dependent lifetime [18].

When a light of certain wavelength is incident on the sample, there is emission of photons depending on the intensity of the emitted light, which effects the number of the excited states. This change in the excited states is mathematically given by,

$$\mathrm{d}N = -\beta N \ \mathrm{d}t \tag{2.1}$$

where, $\mathrm{d}N$ is the changed excited states, β is the rate constant and $\mathrm{d}t$ is the elapsed time. Integrating eq.(2.1), we get

$$N = N_0 e^{-\beta t} \tag{2.2}$$

where N_0 is the initial number of excited stated. Differentiating eq.(2.2), we get,

$$\frac{\mathrm{d}N}{\mathrm{d}t} = -\beta N_0 e^{-\beta t} dt \tag{2.3}$$

Here, the intensity I of the emitted light is given by $\frac{dN}{dt}$, $I_0 = \beta N_0$ is the initial intensity. The negative sign shows that the intensity is decreasing with time. Hence,

$$I = I_0 e^{-\beta t} \tag{2.4}$$

Taking logarithm on both sides and rearranging, we get-

$$ln\left(\frac{I}{I_0}\right) = -\beta t \tag{2.5}$$

Comparing above equation with $y = mx + c$, we see that $-\beta$ is given by the slope of the straight line in equation (2.5). The inverse of this slope is defined by the lifetime decay (τ), where $\tau = \beta^{-1}$ [19].

2.1.3 Luminescence

We might have seen materials glowing due to high temperature or due to radiation, however, luminescence is different. It is created sources apart from heat and is observed when the electrons from lower energy state are excited to the higher energy state along with the emission of light. Many types of luminescence have been observed by the researchers like triboluminescence, bio-luminescence, chemo-luminescence, photoluminescence and many more. Here, photoluminescence is our interest of study. Luminescence induced by light energy is termed photoluminescence and is formally divided into two categories: fluorescence and phosphorescence. They both are similar, however, different in the sense that phosphorescence has longer excited life time than fluorescence. Also, phosphorescence is observed during the excitation and fluorescence is observed after the excitation. Since, the interest is to observe the intensity of the excitation, phosphorescence is the one that is usually used for finding the temperature in a thermographic phosphor system.

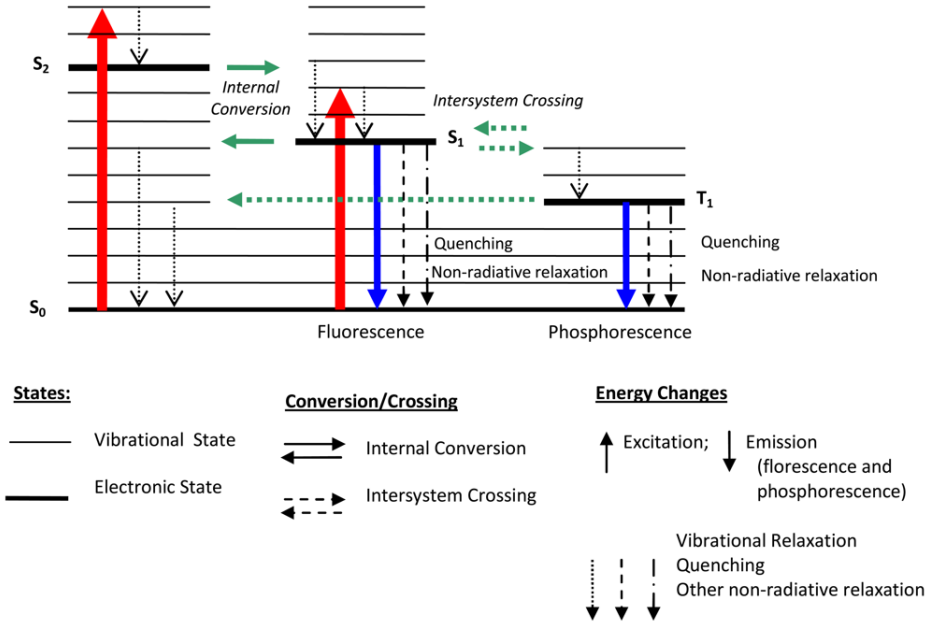

Figure 2.1: Jablonski energy level diagram showing luminescence process [17].

To make it easier, in 1888 the term luminescence was introduced by Eilhard Wiedemann that includes all light emission including both fluorescence and phosphorescence. Regardless, these two terms are still a subject of discussion [17].

We know that the excitation by a light of certain wavelength makes the electrons to jump to the higher states. However, they cannot remain there for a long time. The vibration, relaxation, internal conversion, intersystem crossing, and emission happens soon causing the excited electrons to come back to the ground state giving the glow to the materials which can be shown by the Jablonski diagram in Figure 2.1.

2.2 Thermal Conductivity

There are different means and modes for the transfer of heat energy like electrical carriers lattice waves, electromagnetic waves or other excitation in solids. However, in solids, the electrical carriers carry the majority of the heat in metal whereas lattice wave dominant in insulators [20]. Thermal diffusivity and specific heat including thermal conductivity are used to describe the heat transport through a material [21]. Here, we are focusing on the thermal conductivity of our material.

Thermal conductivity is defined as a property that indicates how fast heat is conducted through a material [22]. Normally, the total thermal conductivity K can be written as a sum of all the components representing various excitations.

$$K = \sum_i K_i$$

where i is the excitation. Depending on the magnitude and temperature, K values of solids vary from one material to another. Differences in sample size, grain size, lattice defect, and dislocation may be the reasons behind the variations of κ value. Mathematically,

$$\kappa = -\frac{Q}{\nabla T}$$

where Q is the heat flux and ∇T is the temperature gradient [20]. Thermal conductivity, among the thermal properties of insulation materials, is considered as the most significant as it directly affects the resistance to transmission of heat (R-Value) that the insulation material must offer [23].

Different methods like transient hot wire(THW), transient line source (TLS), transient hot strip (THS), and Transient Plane source (TPS) are used for the measurement of the thermal conductivities of the isotropic and the homogeneous materials [21]. In this work, we have measured the thermal conductivity of our sample by TPS technique.

2.2.1 Transient plane source (TPS) Technique

TPS technique also known as the "hot disk" is a very appropriate way for characterizing the K values of materials [23]. The measurement with this technique is generally applied to the materials that are considered as insulators and is conducted with a guarded-hot-plate apparatus [24].

Two flat samples of identical area, density and thickness are placed on the opposite side of the probe. The probe is made up of Nickel metal double spiral and is supported by a thin kapton film to protect the shape, provide mechanical strength and to keep it electrically insulated. Current passing through the sensor increases the temperature of the samples and thermal conductivity is calculated on the basis of time dependent temperature increase [25].

For a hot disk sensor that is electrically heated, the resistance increases as a function of time and can be taken from the temperature coefficient equation:

$$R(t) = R_0[1 + TCR(\Delta T_0 + \Delta T_{avg})] \tag{2.6}$$

This equation can be rewritten in terms of the total temperature change as

$$\Delta T_t(t) = \frac{1}{TCR}\left(\frac{R(t)}{R_0} - 1\right) \tag{2.7}$$

where TCR is temperature coefficient The total change in temperature recorded by the sensor produces a response curve as shown in Figure 2.2, with

$$\Delta T_{avg} = \Delta T_t(t) - \Delta T_0 \tag{2.8}$$

The time dependent temperature increase is dependent on sensor radius and output power, provided by the Therm Test reference manual is [25]

$$\Delta T_{avg}(t) = \frac{P_0}{\pi^{\frac{3}{2}}}\frac{1}{r^2\kappa}\sqrt{\frac{t}{\alpha}} \tag{2.9}$$

The hot disk sensor simultaneously reads the values for $\Delta T_t(t)$ and $R(t)$ over the time of the measurement. Manually, the measurement time and output power are set. Thermal conductivity was then solved for by an iterative

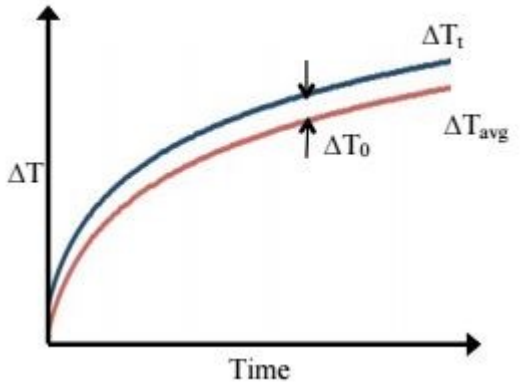

Figure 2.2: Total and average temperature response curves of a TPS sample process using equations (2.7) and (2.8).

2.2.2 Modeling of thermal conductivity in composites

There are two models that were followed while taking the measurements for the K values, series model and parallel model.

The parallel model assumes there is contact between the particles. In the parallel model, each phase is considered to contribute independently to the total conductivity, proportionally to its volume fraction as shown in equation (2.10).

$$K_c = K_p.\phi_p + K_m.\phi_m \tag{2.10}$$

where, K_c, K_p, K_m are the thermal conductivity of the composite, particle, matrix respectively and ϕ_p, ϕ_m are the volume fractions of the particles and matrix respectively. Now, the series model assumes that there is no contact between the particles and the conductivity of the composites in this model

is given by,

$$K_c = \frac{1}{\left(\frac{\phi_m}{K_m} + \frac{\phi_p}{K_p}\right)} \tag{2.11}$$

According to the literature published before, most of the values obtained for the K usually falls within these two models [26].

2.3 Mechanical Test

Every material has a limited strength, and the strength is determined by its rigidity or elasticity. PDMS is an elastic and soft material and that is the reason it can be easily used for reversible deformations needed during the analytical operations. PDMS has the property of bonding to itself and/or to other surfaces creating a watertight seal. Using this property, PDMS membranes with different thicknesses can be used to form various three-dimensional microstructures such as micro-channels and micro-chambers. PDMS is generally considered as a bulk but this is not always the case, as the thickness decreases we should understand whether or not it makes PDMS membranes dimensional dependent [27].

Recent microfluidic and micro electro mechanical systems have shown that the high elastic properties of the PDMS has provided distinct pros over conventional materials like glass, silicon and harder materials. This increasing no of advantages of elastic substrate of PDMS has provided a reason to look for its mechanical properties [28].

Here, we are trying to observe how the addition of powder in the elastomer will change the mechanical properties of the PDMS doped by weight.

2.3.1 Tensile Testing

Different samples of PDMS were prepared in different rpm to investigate the mechanical properties of PDMS films with different mixing ratios of the base polymer and curing agent. As the samples are easily affected by various natural factors like tensile, compression and shear stress, they need to be considered in materials selection for mechanical design. Also, we should not neglect the time and temperature conditions.

All of our tests for the tensile were done in the room temperature. Testing stress and strain of PDMS helps us know the strength of the substance. This test is a destructive method in which we cut our specimen to a dog bone shape to a standard size.

The strength of phosphor doped Sylgard 184 is known by interpreting the Young's Modulus from the slope of a stress-strain curve after doing the linear fit in the curve. It is also defined as the ratio of stress to the strain, i.e.

$$\text{Young's Modulus } (Y) = \frac{\text{Stress}}{\text{Strain}}$$

Where, stress is the ratio of force to cross-sectional area and strain is the ratio of change in length to the original length.

Chapter 3

Materials and Methods

3.1 Sample synthesis and preparation

For the conduction of our experiment, we have prepared different kinds of samples with different thickness. This includes the samples prepared using Sylgard 184 Silicone with Lanthanum Oxysulphide (La_2O_2S:Eu), commonly known as phosphor only and silicone with phosphor and carbon. For both case, we have samples made in single layer and samples made in multiple layer. The method applied to prepare these samples is almost the same but however differs slightly.

3.1.1 Single-layer single-concentration La_2O_2S:Eu/Sylgard 184 composites

There were two different batches of Lanthanum Oxysulphide (La_2O_2S:Eu) that were used while preparing the samples. The first batch used was 23010 SKL63/F-X La_2O_2S:Eu with 0.1m/o %Eu, and the second batch of sample used for the preparation of sample was from lot 23015 SKL63/F-A1 La_2O_2S:Eu doped with 1m/o %Eu.

For different measurements like thermal conductivity, mechanical test and fluorescence, single sided drop cast samples were prepared without using the phosphor (Neat Sylgard) and using the phosphor from two different batches (SKL63/F-X:0.1% Eu and SKl63/F-A1:1%EU). No thin films or multilayered

samples were prepared.

For this, Sylgard 184 and cross-linker were mixed in the ratio 10:1 i.e. the guidelines provided by the manufacturer (Dow Corning, Midland, MI). Then the required amount of La_2O_2S:Eu powder by weight was added to the mixture and was stirred with a metallic spatula until it got mixed thoroughly. All of the measurements were done in Fisher EMD XE Series Model 100A microbalance. The mixture was poured into a very thin flat surface of aluminum pan and then outgassed in a Precision M-3 Scientific vacuum oven at room temperature until the mixture had no air bubbles remaining and finally left for curing in Cascade Tek oven from TEK for 1 hour at 80°C. Then the samples as shown in Figure 3.1 and 3.2a were peeled from the substrate.

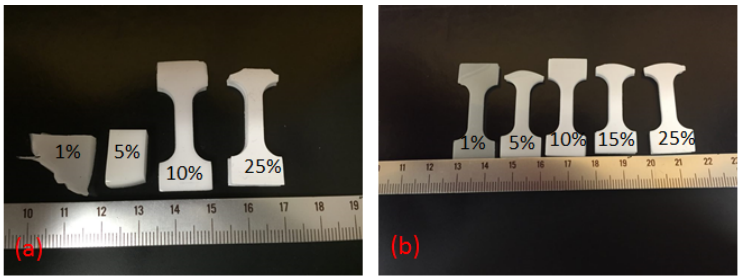

Figure 3.1: Samples prepared from two different batches (a)SKL63/F-X with 0.1 % Eu and (b) SKl63/F-A1 23015 with 1 % Eu

1, 10 and 25% doped PDMs was cured using the phosphor with 0.1% Eu. Whereas phosphor with 1% Eu was used to synthesize 1%, 5%, 10%, 15%, 20%, and 25% doped PDMS. Samples of PDMS doped in different concentration with just phosphor (La_2O_2S:Eu) were prepared.

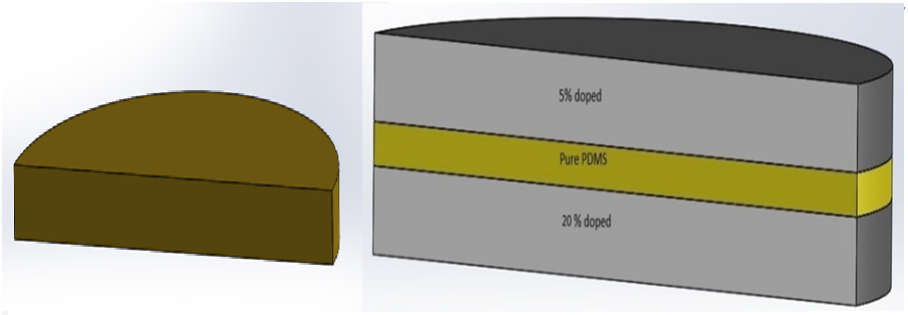

Figure 3.2: Schematic diagrams of (a) single layer composites and (b) multi-layer composites

3.1.2 Multi-layer multi-concentration La_2O_2S:Eu /Sylgard 184 composites

We have prepared three different types of multilayered samples, namely 15-P-5, 15-P-10 and 5-P-20 spun in 0, 500, 1000, 2000, and 3000 rpm. Figure 3.2b shows a schematic diagram of the multilayer structure created, where the Neat Sylgard184 layer is sandwiched between two layers of Sylgard 184 with different concentrations of La_2O_2S:Eu.

For this, the Sylgard 184 and cross-linker were added in the ratio 10:1 as mentioned in section 3.1.1 and required amount of phosphor were added together, outgassed and spin coated at 500, 1000, 2000 and 3000 rpm for each required concentration in Chemat Technology Spin-Coater KW-4A, again outgassed and finally left for curing in oven for 1 hour at 80°C.

Similarly, Neat Sylgard mixture (no powder) was prepared and poured onto the top of the same sample previously prepared, it was cured and finally another same powder doped mixture of different concentration was cured onto the top of the same sample. The samples as shown in Figure 3.3 were then carefully peeled out from their supporting surface.

Similar to the thin film 2 sided, the drop cast ones were prepared in the

same way followed by the mixture of Sylgard 184 and cross-linker in the ratio 10:1 and mixing of phosphor by weight and outgassing. But instead of spin coating, PDMS doped with definite X concentration is cured first in the petri dish. After that, Neat Sylgard is cured on top of that and finally PDMS doped with Y concentration is cured. In this way, 15-P-5, 15-P-10, 5-P-20 samples were made in 0 rpm.

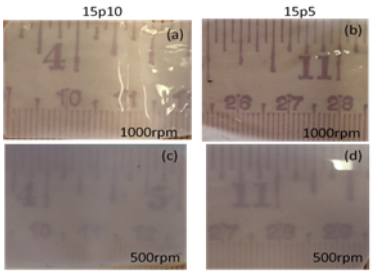

Figure 3.3: Multilayer doped PDMS spun in 1000rpm (a and b), and in 500rpm (c and d).

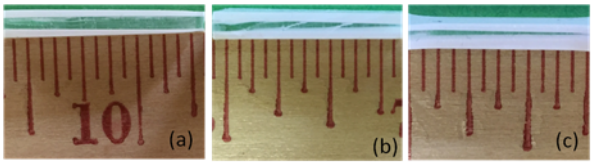

Figure 3.4: Multilayer doped PDMS spun in 0rpm showing thickness gradient

3.1.3 Carbon/ La_2O_2S:Eu /Sylgard 184 composites

Both the drop cast and the thin films were synthesized using the carbon, silicone and phosphor. To increase the conductivity of the sample was the reason behind using carbon powder along with the phosphor.

There were three kinds of thin films prepared. The first one includes 50% carbon and 50% phosphor by weight doped PDMS, the second includes 1%

carbon and 99% Phosphor, and third includes 5% carbon (same for all) and phosphor required by weight doped PDMS. We also had prepared 1%, 10% and 25% phosphor along with 5% carbon (amount of carbon same for all) doped PDMS in 2000 rpm.

3.1.4 Preparation of 5% Carbon doped (thin and drop cast) PDMS

To synthesize these samples, we follow the same instructions given by Dow Corning, Midland, MI, that is mixing the silicone and the cross-linker in the ratio 10:1 respectively. However, the way of encapsulating the carbon and phosphor powder is different.

We had prepared 1%, 10% and 25% Carbon mixed samples both in 0 rpm and in 2000rpm. In the mixture of the silicone and cross-linker, 5% Carbon by weight is added to the mixture and then the required amount (1%,0.10%,0.25%) of the phosphor by weight is added. After the proper stirring, the mixture is outgassed and placed in oven for 1 hour at 80°C to get cured. Finally, samples as shown in Figure 3.5 were prepared.

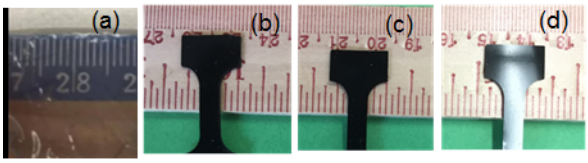

Figure 3.5: Carbon doped thin film doped with 1% carbon(a) and with 5% carbon with 1(b),10(c) and 25%(d).

Preparation of the sample is not only limited to their synthesis. Getting them in the desired shape according to the nature of the measurement technique is also a part of preparation. We did a mechanical test, thermal test,

luminescence test and even did SEM imaging for them, and for each test the synthesized samples needed to be prepared in proper shape and sizes.

3.1.5 Sample preparation for Scanning Electron Microscope (SEM) imaging

To make a sample that can be used for SEM is an interesting work. The SEM samples needed are mounted on a SEM stub. Sputter coater from Electron Microscopy Sciences was used to sputter coat the samples with gold. The samples were coated with 99.99% pure gold (60mm in diameter $\times$ 0.01 mm thick) from Electron Microscopy Sciences, with a thickness of 10nm. All the samples were then viewed with the Scanning Electron Microscope (SEM) from Phenom Pure.

3.1.6 Sample preparation for Optical microscopy

Different samples spun in different rpms (0, 3000) were used to take the optical images. The Accu-Scope Unitron microscope was used to capture the optical images of the thin films using 319CU 3.2M CMOS S/N:141020 microscopes digital camera. The thin film has the Neat Sylgard sandwiched between two different layers of PDMS doped with different amount of phosphor. So, for the same sample the image had been taken twice. The Micrometrics SE Premium image software was used to analyze the images. Using this software, different functions like brightness, contrast, exposure were played with until the phosphor particles were seen easily against the Sylgard 184 background. Since we have multiple layers, to be sure that we are on the right side of the sample, a mark was made on the side which we were trying to focus on. After, taking the image of one side, then the side was flipped and images were taken following the same procedure. The scaling was done manually using the same micrometrics software.

3.1.7 Summary

To summarize, the tree diagram shown in Figure 3.6 describes the samples that had been prepared while doing the research.

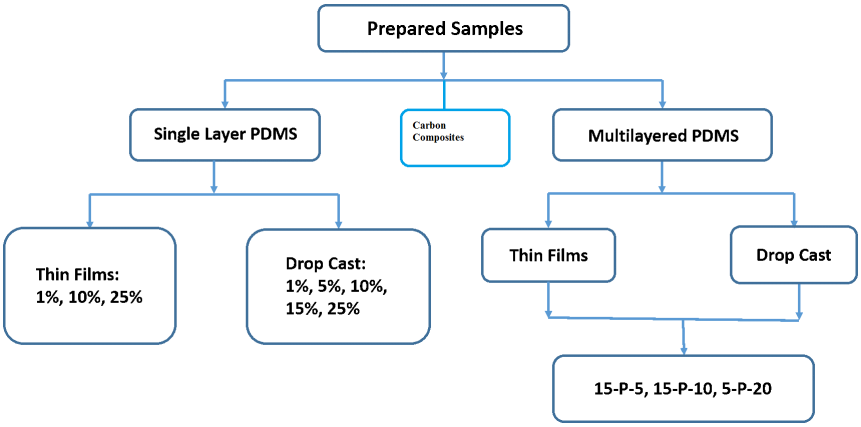

Figure 3.6: Flow diagram showing the various samples prepared for this study

3.1.8 Thickness Measurement of the Sample

The samples, as were prepared in different rpm, maintain different thickness which imply different methods to measure the thickness of them. For the drop cast sample, the thickness was measured directly by the Vernier Calipers. Five different measurements were recorded and then averaged out. But the same could not be applied for the thin films. So, to overcome this, micrometer screw gauze from Mahr GmbH Esslingen Type 40 was used to measure the thickness of the thin films. The thin samples were sandwiched between two identical microscopic slides and the measurement was taken for 5 times and averaged out. Then the thickness of the two slides were deducted from the averaged value which gave us the thickness of the sample.

3.1.9 Sample percentage preparation

It has been explained that most of the samples prepared were using phosphor, however, the amount of phosphor needed to be added had not been explained. Simple mathematical concept like ratio and proportion had been the basis of calculation. For any amount of doping, the silicone and cross linker were added in the ratio 10:1, and suppose the amount made is x gm. Now if we want to make y% doped sample, then the following formula was applied to calculate amount of phosphor needed to prepare y% doped sample,

$$\frac{z}{x+z} = y\%$$

where the amount of x and y is known. By doing algebra z was calculated which would be the amount of phosphor needed to prepare y% doped sample.

3.2 Sample Characterization and testing

3.2.1 Thermal Conductivity measurements

Only drop cast single sided PDMS samples were used to measure the thermal conductivity. Knowing the K values for the thin films would have interesting, however, the samples need to be at least 4 mm thick, so getting k values for the thin films was not done. Starting from Pure (un-doped) PDMS, the experiment was done for 1%, 10%, 25% and 50% La_2O_2S:Eu doped PDMS that comes from the batch of phosphor having 0.1% Eu. All of the measurement were done inside Tenny Junior Environmental Chamber. The transient plane source (TPS) technique was used to collect the K values. 5100 (13 mm) Ni-metal double spiral sensor was used for thermal conductivity measurement in this technique.

The samples were placed above and below the sensor as shown in Figure 3.7a. It should be noted that the size of the sample surface should be larger

than the diameter of the Hot Disk Sensor so that there won't be any shortening of the transient recording. The samples need to be identical too. Hot disk constant thermal Analyzer version 7.1.22 was used to determine the K values. Measurements were done with the TPS 1500 according to the ideal settings for power and measurement time for the materials tested.

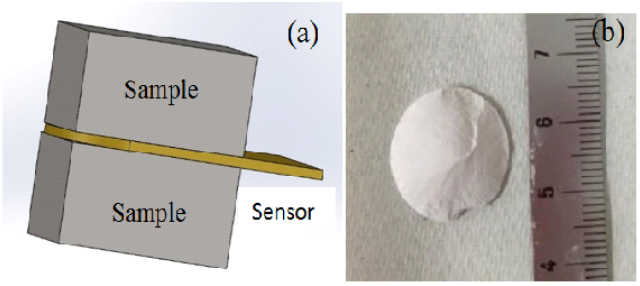

Figure 3.7: Schematic diagram for (a) and (b) measuring thermal conductivity

When the thermal transport measurement is done, there is a flow of electrical current, high enough to increase the temperature of the sensor between a fractions of a degree up to several degrees along with keeping the track of the resistance (temperature) increase as a function of time (11). The measurement was done for 3 times for each of the sample and for each temperature to assess error and uncertainty in the experiment. Also, at least 30 minutes was given for the system to reach thermal equilibrium when the samples were changed. All the data for the specific temperature was then averaged and the graph between the temperature and thermal conductivity was plotted. For the measurement of the thermal conductivity, we needed the samples of definite thickness. The drop cast phosphor doped PDMS were cut to a size of 5X6X5 mm^3. And the measurement was done for 1%, 10%, 25% and 50% phosphor doped PDMS. Also did prepare a pellet of powder by compressing the powder using a carver compressor from Carver Corporation, and the pellet was about 4-5 mm thick.

3.2.2 Tensile Testing

Mechanical test requires its sample in a required shape. The samples were cut in a dog bone shape. The detail description is provided in section 3.2.2.

The tensile test is done to know the strength of the material. Our samples are of different thickness ranging from 0.11mm to 4.5 mm including PDMS doped with just one concentration of phosphor and two different concentration of phosphor. The concept for the drop cast double sided one was to observe whether the application of force going to separate the layers or not.

Before running the test, all the samples were cut into a shape of dog bone following the ASTM standard-ASTM D-1708 test standard as shown in Figure 3.8b.

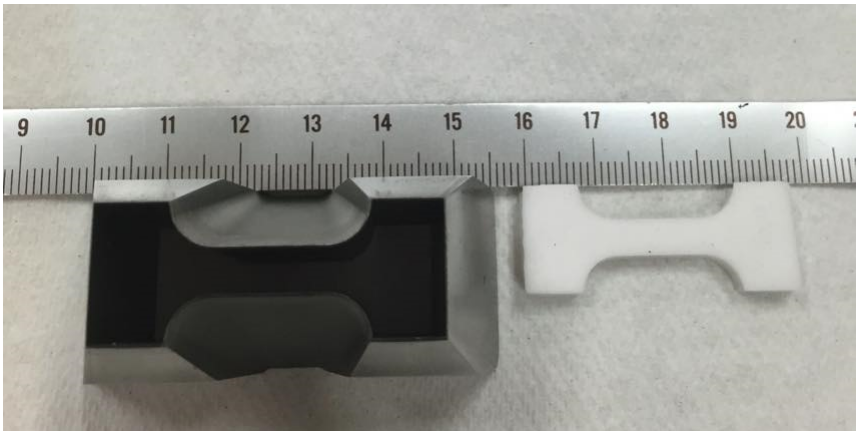

Figure 3.8: ASTM standard dog bone punch(a) and sample(b)

The dog bone punch shown in Figure 3.8a was placed on top the samples and pressed hard and the required specimen was separated from its surface.

We had three samples for each 0, 500, 1000, 2000 and 3000 rpm, and three samples from Carbon with Phosphor doped PDMS and just regular one sided phosphor doped PDMS cut in dog bone shape. Mark-10 from model BG200 bench top tensile tester was used to observe the stress-strain behavior of the samples under the ambient conditions. The tensile tester has the maximum

load of 1.5 kN.

The specimen was placed in the grips of the double clamped gripper and held firmly but not too much tightened [15]. After the installation, a standard test of tensile properties of the samples was performed by slowly increasing stress on the samples from zero to the value at which the specimen fractures with a pull rate of 1 inch per minute with a resolution of 0.01. Mesur gauge software was used to analyze the data. The data was then exported in an excel file and finally the calculation was done. For each sample from different rpm, the Young's modulus was obtained twice and the final Young's Modulus is the average of the two of them.

3.2.3 Luminescence measurements

Here, we were focused on the decay properties of the carbon + phosphor doped thin film PDMS and two sided thin film PDMS. Our aim was to measure the temperature of the surface by observing the luminescent life-time. Fluorescence is observed only if the wavelength of the exciting source is shorter than the emitted fluorescence.

The measurement was supposed to be done at both high and low temperature. However, at the low temperature there is always risk of having layer of frost on the surface of the sample. Because of this, the experiment was conducted inside the environmental chamber. The environmental chamber is a transparent box like structure with a pair of plastic gloves attached with it. Humidity can be controlled inside the chamber. For the measurement we had a desiccator column attached with the Desiccant Pump Dehumidification System MODEL 5471 from ETS connected to the environmental chamber from ETS. The chamber has an inlet and an outlet. From outlet, the humid air goes to the desiccator where the desiccants absorb the humidity and the dry air is again sent back to the chamber through the inlet.

To have the information of humidity, a dehumidifier controller MODEL

5112 from ETS was also connected and the sensor was inserted inside the chamber. Temperature controller MK 1000 from INSTEC a stage was needed in which the sample is placed. The stage has an inlet through which the liquid nitrogen is passed to maintain low temperature. The schematic diagram of the experiment is given in Figure 3.9a.

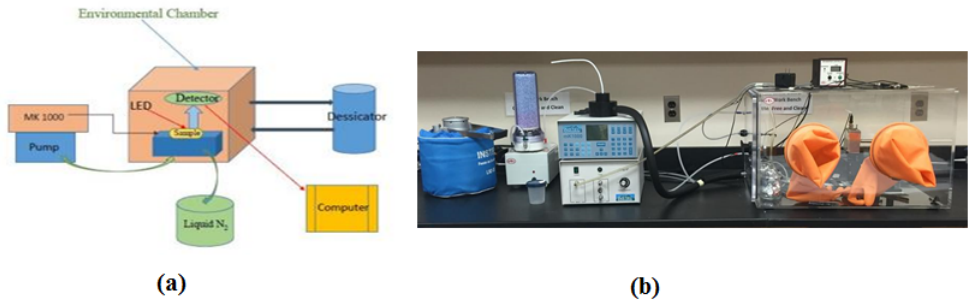

Figure 3.9: Schematic diagrams of test setup in an environmental chamber (a) and (b) actual setup for luminescence measurements.

The setup for testing luminescence consists of 30 mm cage from Thorlabs associated with SM-1 lens tubes and mounting hardware. Light emitting diode emitting 365nm from LED Engine (part no-LZ1-10U600) was specified at 200mW. The LED emission is reflected from a Thorlabs long pass dichroic mirror, part number DMLP425R with 425nm cutoff, after passing through a silica lens L1. There is another silica lens L2, through which the light is focused onto the sample. There we can see luminescence of many visible wavelengths consisting of yellowish orange colors. The luminescence within the collection angle of the L2 lens directs the light back up, vertically and through the dichroic mirror which passes light greater than 425 nm. The third lens L3, is for focusing the light onto the photosensitive surface of a photomultiplier tube (PMT). Then the light of 510+/- 5 nm is transmitted from an intervening pass filter. This allows the 5D2 emission from the phosphor to reach the detector which is very temperature dependent. Then this

optical signal is converted to electrical analog by the PMT, which is then digitized by a Tektronix TDS 2012-C oscilloscope. Finally, the data received by the computer is saved in .csv files, and the calculation was done in EXCEL.

The experiment was performed in two sections. One in high temperature and another in the cryogenic. For getting the decay curve of the sample at a high temperature, the temperature is set on the MK 1000. Once the set number is reached, the decay curve is observed and is saved.

However, the situation is not the same for cryogenic. There should be the regular supply of liquid nitrogen for maintaining low temperature. A separate instrument LN2-P from INSTEC is needed in addition to MK 1000, which pumps the liquid nitrogen from the VAT. Extra care should be given while handling the nitrogen as it is harmful when it is 77K cold.

After the completion of the observation for the double sided thin film, observation for the multilayered thin films and single layered drop cast were done using the same process.

A simple negligence can result in the error as the thin films are very delicate and can stick to any other surface, should be handled carefully. The sample should be in a flat position; elevation should be avoided at its best.

Chapter 4

Results and Discussion

4.1 Luminescence behavior

The temperature dependent luminescence behavior of the single layer and multilayer samples prepared for this study are presented in this section over a wide range of temperatures, as shown in the graphs below.

4.1.1 Single layer

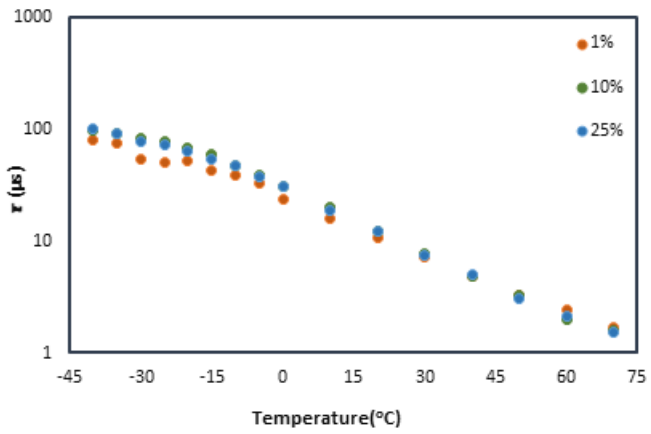

Figure 4.1: Luminescence of single layer drop cast PDMS

The temperature dependent luminescence decay characteristics of the 1%, 10%, 25% drop cast single layer composite samples are shown in Figure 4.1. Measurements were taken from -40 °C to +70 °C in a continuous sweep allow-

ing for thermal equilibrium to be reached at each temperature, for each sample tested. At lower temperatures, the decay times are significantly higher than those measured at high temperatures and as the temperature increases, the decay times become shorter and shorter, as expected and observed previously [29]. The low temperature decay behavior is consistent with previous studies measured for the powder only [30]. The decay time constant is not expected to have any dependency on the concentration level of the powder itself, as long as the intensity of the emission signal detected is above noise level for the instrumentation and test setup used. The measured time constants for all three concentrations 1, 10, and 25% do in fact appear to be very close at each temperature and independent of the concentration level. The slight discrepancy between the values reported for the 1% sample and the 10% and 25% is attributed to experimental error inherent to making such measurements. Overall, the results show that the sensitivity to temperature is dramatic. For instance, for the 1% dropcast sample data depicted in Figure 4.1 the decay time at 10°C is 15.8 μs and at 0°C it is 23.6 μs. This is a change of 50% in only 10 degrees.

4.1.2 Multilayer: Dropcast and 2000 rpm

The temperature dependent decay profile of the multilayer samples was also characterized for both the drop cast (0 rpm) (Figure 4.2) and 2000 rpm samples (Figure 4.3). Once again the samples were tested from -40 °C to +70 °C

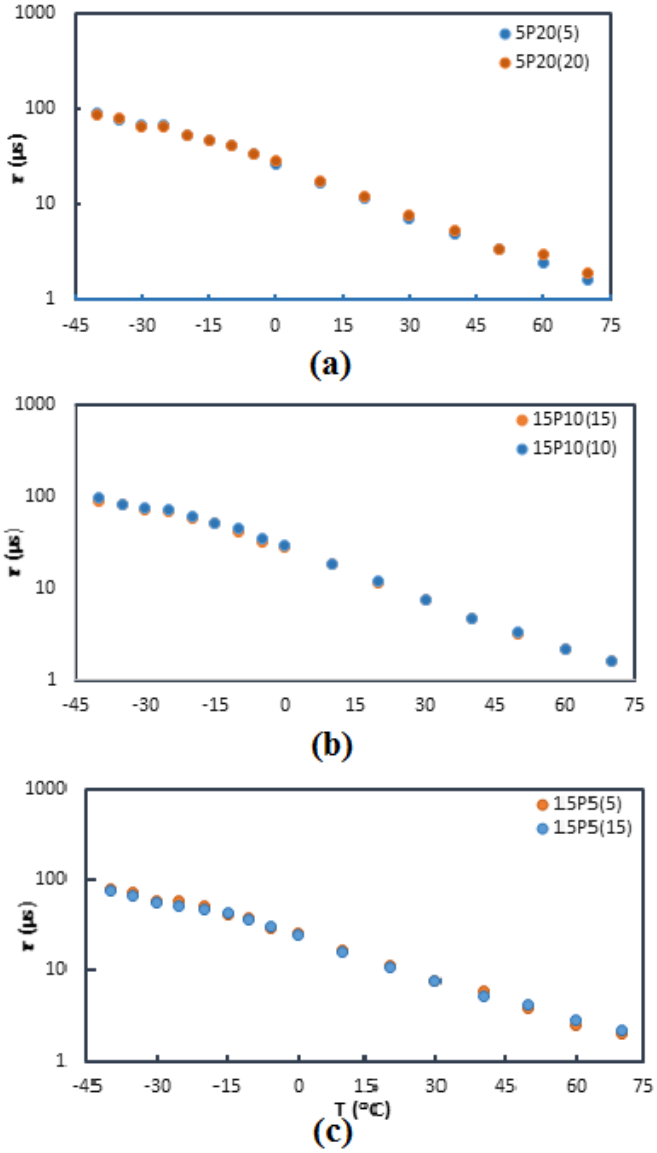

Figure 4.2: Luminescence of multi-layer drop cast doped PDMS

in a low humidity environmental chamber as previously described. The decay constants for drop cast 15P10, Figure 4.2(a), 5P20 Figure 4.2(b), and 15P5 Figure 4.2(c) samples follow a similar trend to that observed for samples in Figure 4.1 meaning that as the temperature rises the decay time decreases

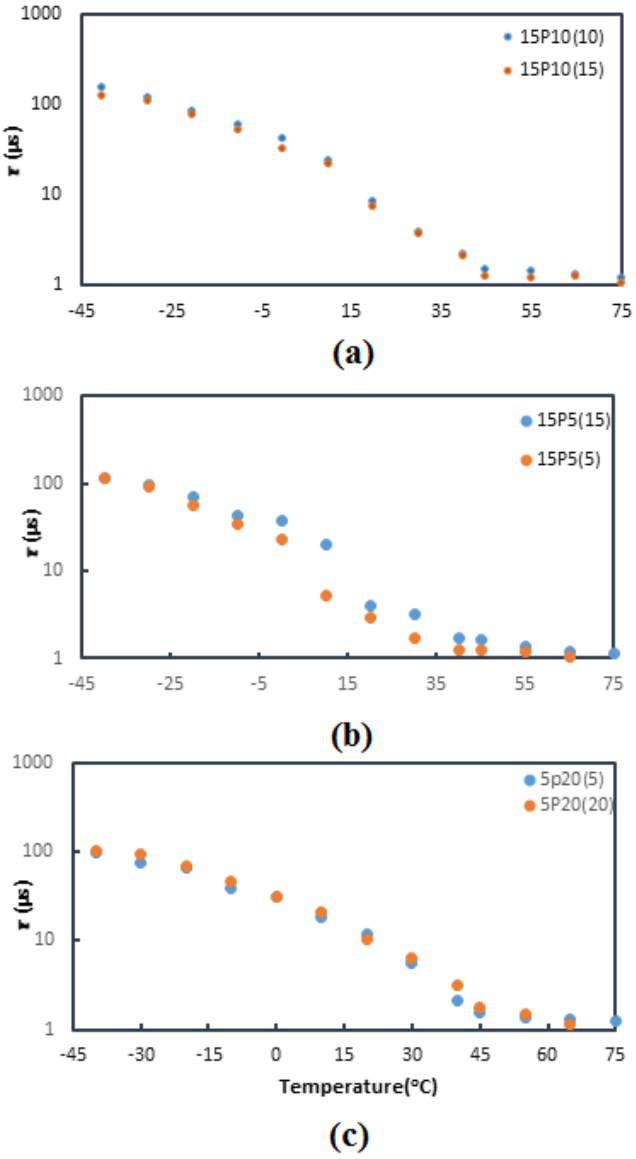

Figure 4.3: Luminescence of multi-layer 2000 rpm doped PDMS

substantially. In spite of the insulating layer of Neat Sylgard sandwiched between the two composite layers, a significant change in the decay time constant of the two sides was not observed for any of the samples tested suggesting that a detectable temperature gradient did not exist. The decay behavior of the multilayer samples at 2000 rpm similarly did not show a temperature gradient across the sample, not surprisingly, since the 2000 rpm samples would have reached thermal equilibrium faster than the drop cast samples (0 rpm) of Figure 4.2. Additionally, at 2000 rpm the samples appeared optically transparent and it is quite likely that exciting once side of the composite structure inevitably lead to excitation and hence emission from the opposite side also. No noticeable differences were detected in the emission behavior of the 0.1% and 1% Eu batch of phosphor powders acquired. Samples thinner than the 2000 rpm were difficult to handle and were not tested for this region.

4.2 Tensile properties

4.2.1 Single Layer

The tensile properties of single layer samples prepared for this study are presented here.

In our discussion we are assuming a uniform and homogeneous particle distribution and dispersion.

The effect of La_2O_2S:Eu powder concentration on the tensile properties of the composite polymers was evaluated and is shown in Figure 4.4 both for the 0.1% (Figure 4.4a) and 1% Eu (Figure 4.4b) concentrations. As the concentration of the La_2O_2S:Eu (0.1%) increased from 1 wt % to 25 wt % the composite material became stiffer, by a noticeable change in its Young's modulus (Figure 4.5) which has been observed previously and is supported

by published literature [31][32][33][34]. In the case of La_2O_2S:Eu (1.0%) however, an increase in powder concentration from 1 to 25 wt % surprisingly did not lead to a noticeable change in Young's modulus (Figure 4.5), and, at low strains the values remained very close to one another. At higher strains however (nonlinear region of Figure 4.4b) a slight dependence on concentration levels did begin to appear. Tensile testing was terminated prior to rupture of samples.

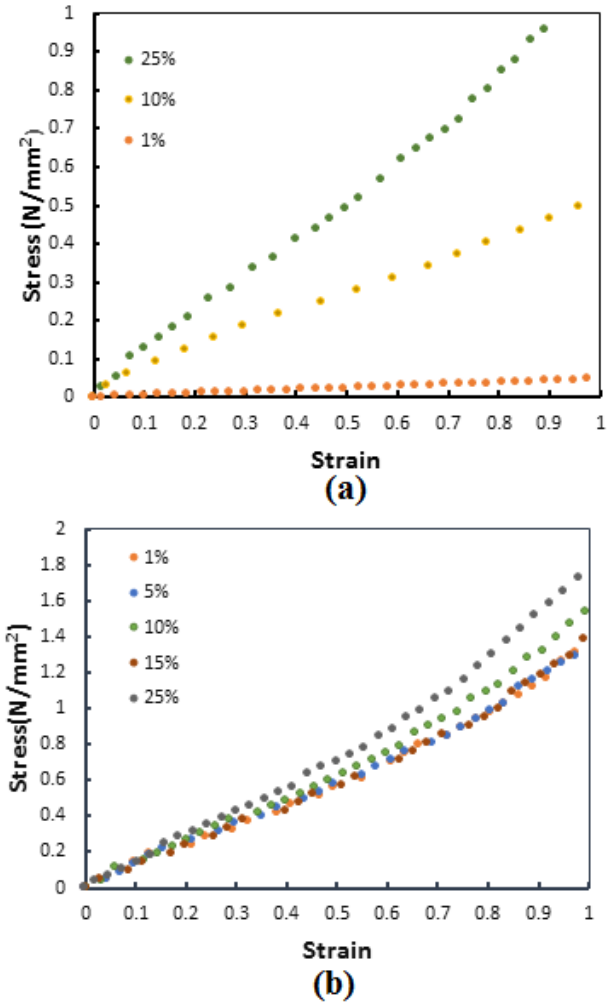

Figure 4.4: Stress-strain curve of 0 rpm with 0.1%Eu(a) and with 1% Eu(b) as a function of concentration

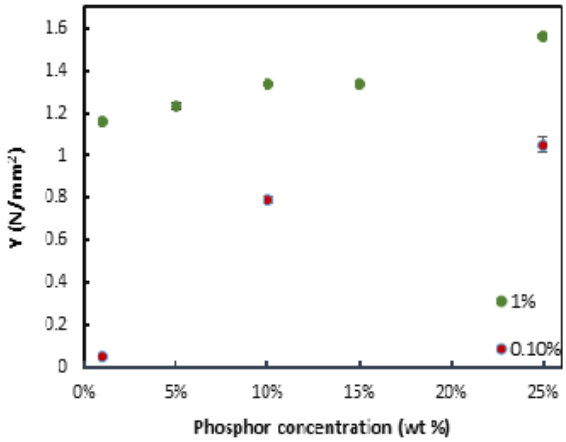

Figure 4.5: Young's modulus as a function of concentration

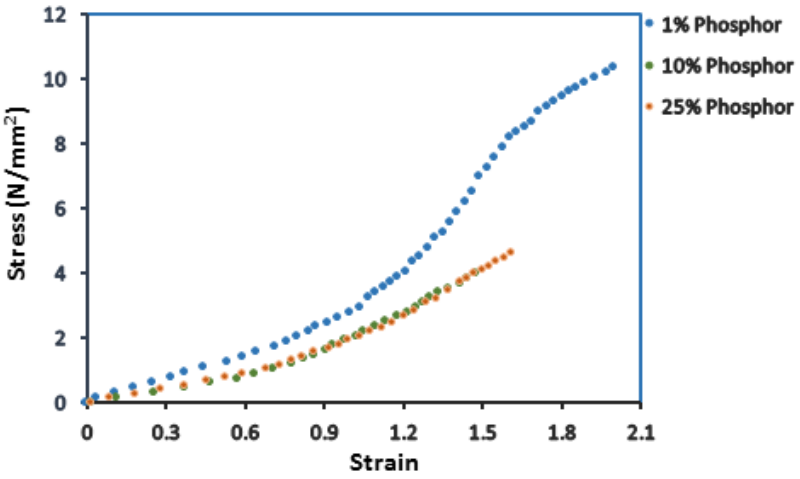

Figure 4.6: Stress-strain curve of carbon doped PDMS with 5% carbon

Similarly, the effect on the tensile properties of the composite polymer with the addition of the carbon powder along with La_2O_2S:Eu which is shown in Figure 4.6. From the Figure 4.6, it is seen that the Neat Sylgard with 1% of phosphor is more elastic than 10 and 25%.

4.2.2 Multilayer

The tensile properties of the multilayer composites prepared in this study are presented here.

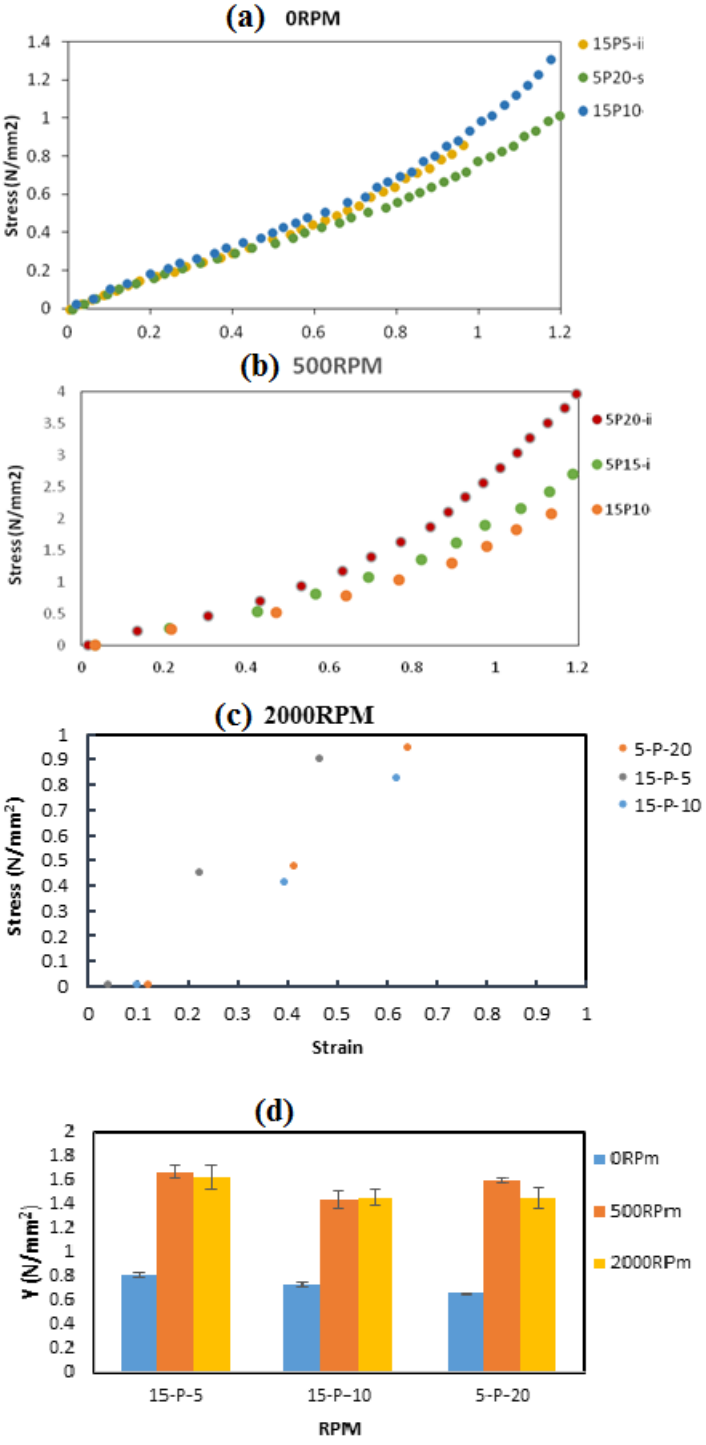

Figure 4.7: Stress-strain curve of multilayer thick (a), thin films (b and c) and their Young's modulus (d) as a function of concentration.

The tensile properties of the multilayer PDMS+La_2O_2S:Eu (0.1%) composites are shown in Figure 4.7 for 0 rpm (Figure 4.7 (a)) 500 rpm (Figure 4.7b), 2000 rpm (Figure 4.7c), and comparision of Young's Moduli for different rpm (Figure 4.7(d)). At low strains the differences in the tensile behavior of the 3 layers combined is not noticeable. However, at higher strains differences in the multilayer tensile properties become more prominent. Given that interfacial bonding between particles and PDMS matrix is not expected to occur due to the polymer's low surface energy [35][36] leading to an absence of stress transfer, the differences in the tensile profiles is attributed to the differences in particle distribution. As the spin speed was increased it was discovered that the multilayer composite polymers became stiffer, by the same amount, and weakly dependent on the actual layer structure (Figure 4.7c). The stiffening effect observed here as a function of rpm has been observed previously [15] for neat PDMS and described as"dimension dependent" change in tensile properties when transitioning from bulk samples to thin samples prepared by spin coating techniques.

Figure 3.1.2 shows optical images of the 500 rpm and 1000 rpm multilayer samples and that at 500 rpm and above as the film thickness is reduced the composite samples appear clearer and clearer. Non uniformities in the drop cast film thicknesses (shown in Figures 3.4a and 3.3b) across the length of the dog bones prepared could lead to inaccuracies in the tensile behavior of the multilayer samples created. For very thin samples (e.g 3000 rpm) we were not able to collect reliable tensile profiles due to slipping of the specimen through the grips. At 1000 rpm and above all multilayer samples were optically transparent while below 1000 rpm (500 rpm and below) the samples showed a degree of translucency due to scatter from the powder particulates. All drop cast samples (0 rpm) were opaque. In some studies, more than 5% wt. loading content particle aggregation occurred leading to composite strength degradation [37].

4.3 Microscopy results

4.3.1 Scanning Electron Microscope (SEM) results of La_2O_2S:Eu powder

Scanning Electron Microscope images of the La_2O_2S:Eu (0.1% and 1%) in powder form revealed a noticeable difference in grain size, as seen in Figures 4.8a and b for the 0.1 % powder and in 4.8c and (4.8f for the 1% powder. In addition to the size differences, the 0.1% powder formed clusters, which we associate with the presence of a high electrostatic charge, while the larger particulates of the 1% powder do not appear to form large clusters. The 1% powder has much larger particles than the 0.1% as can be seen from the SEM images. Also, it can be seen that in the case of the smaller particles of 0.1% they are sticking together in large numbers and this is attributed to the electrostatic charge present and it is most likely contributing to the cluster formation and "towering" that is observed (Figure 4.8d arrows). This type of accumulation has been observed previously with other μm-sized charged particles [33]. The compression of the powder with the Carver did not affect the grain size as can be seen in Figures 4.8b and 4.8e, which is an image of the 1% powder after compressed into a pellet form.

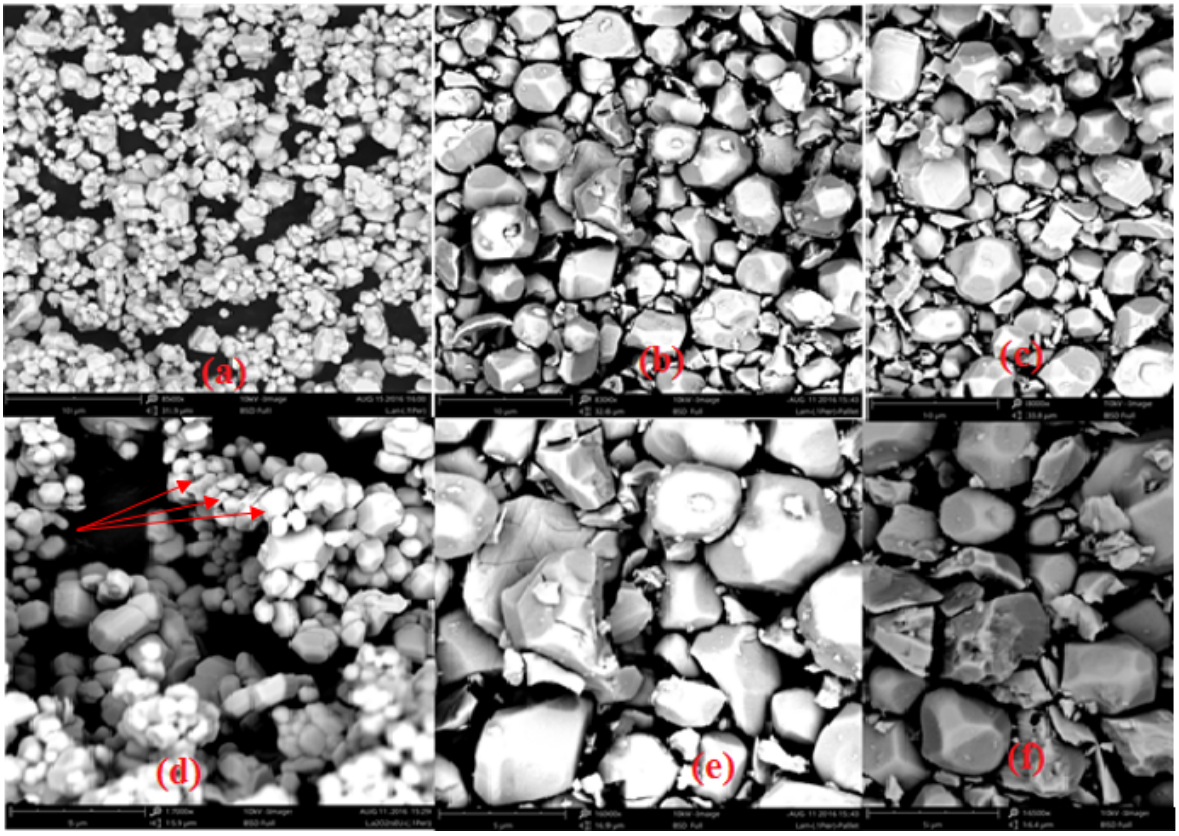

Figure 4.8: SEM image for just La_2O_2S:Eu (a) and (b) with 0.1%Eu, (c) and (d) pallet powder with 1%Eu, (e) and (f) with 1% Eu.

4.3.2 SEM of Carbon powder

The SEM image of the carbon powder shown in Figure 4.9 shows a huge difference when compared with the SEM of the powder shown in figure 4.8. The cluster size is bigger than the 0.1% powder shown in figure 4.8a which contributes to the electrostatic charge. This change in the morphology of the powder agrees well with the different result obtained for the carbon and phosphor tensile test.

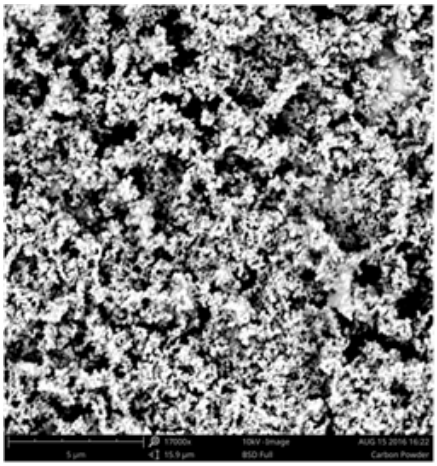

Figure 4.9: SEM image for carbon powder

4.3.3 Optical Microscope results

Figure 4.10 shows the optical images of multilayer sample from two different rpm, 0rpm (Figure 4.10a) and 3000rpm (Figure 4.10b). These images show the distribution of the La_2O_2S:Eu powder encapsulated inside the Neat Sylgard as a function of rpm. Both of the samples were observed with a magnification 10X. There is high distribution of the particles in 3000rpm sample and the particles seem to be in compact form in 0 rpm sample.

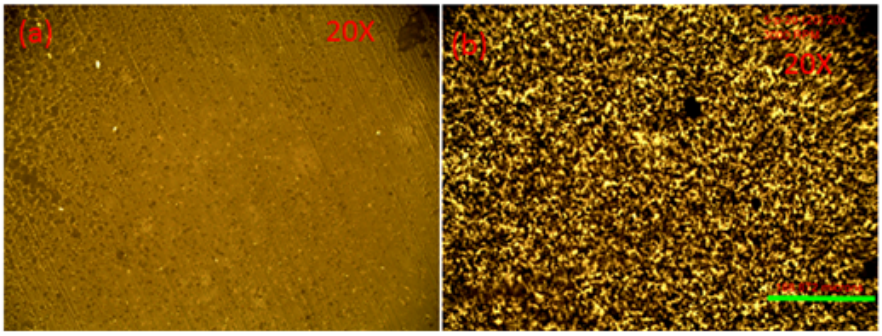

Figure 4.10: Optical image of 0 rpm sample (a) and 3000 rpm sample (b) taken at magnification of 20x

4.4 Thermal conductivity

This section describes the results we obtained for the thermal conductivity of the composite samples we prepared here.

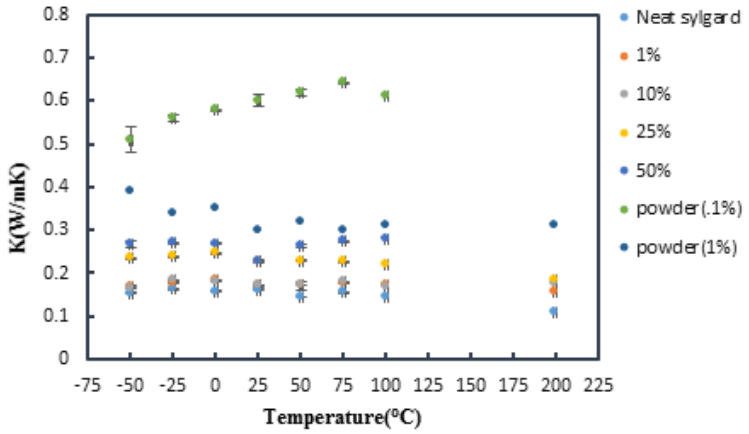

Figure 4.11: Thermal conductivity as a function of concentration

The thermal conductivity of the composite polymers was measured between -60 °C and 200 °C, in increments of 20 °C and is shown in Figure 4.11. The thermal conductivity of Neat Sylgard 184 (without phosphor powder added) compares well with other published literature [37]. For pure La_2O_2S:Eu powder no published literature was available. Both the 0.1 % and 1 % powders were measured. The thermal conductivity of the powder only did not appear to be strongly dependent on temperature, in the range studied here. However, the 0.1 % powder generally had a higher K value than the 1.0% powder. This could in part be due to the fact that the grain size of the 0.1 % powder is smaller and as a result forms a more compact pellet, with less air space between the grains while the 1% powder has large grain sizes and as a result allows for more air space between particles and consequentially shows a lower K value. The measured K values for the 1%,

10%, and 25% composite polymers were greater than the K value for pure Sylgard 184, and, less than pure La_2O_2S:Eu (100% powder) K value. Each measurement is an average of 3 independent measurements for each sample, at each temperature.

4.4.1 Modeling of thermal conductivity in composites

Table 4.1: K values calculated using parallel and series method

Thermal Conductivity(W/mK) at RT					
Powder Concentration (wt %)	Parallel Method (1%)	Parallel Method (0.1%)	Series Method (1%)	Series Method (0.1%)	Measured Value
0%	0.161	0.16	0.161	0.16	0.16
1%	0.162	0.16	0.162	0.16	0.17
10%	0.175	0.20	0.169	0.17	0.17
25%	0.196	0.27	0.182	0.2	0.23
50%	0.231	0.38	0.210	0.25	0.23
100%	0.301	0.6	0.301	0.6	0.3

The two accepted basic models representing thermal conductivity of composites are the rule of mixture of parallel model and the series model [26]. In the parallel model each phase is assumed to contribute independently to the overall thermal conductivity of the composite and assumes perfect contact between particles in the matrix. In the series model however no contact between particles exists. Most experimental results fall in the region between what the two models predict [26]. Table 4.1 shows the calculated k values using parallel and series method and Figure 4.12 shows a plot of the calculated series and parallel model values for our composites and compared with

the experimental values measured at room temperature. The experimental values obtained at room temperature do indeed mostly fall in-between the values obtained from the series and the parallel models.

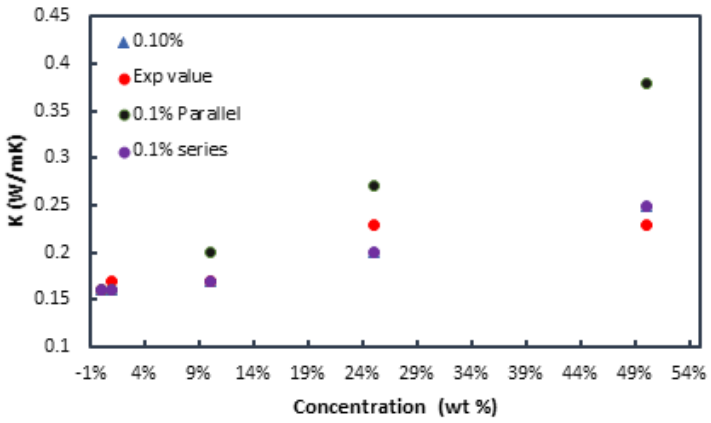

Figure 4.12: Comparison of the measured K values with calculated K values

4.5 Thickness measurements

The thickness of the samples prepared in different rpm had been measured which is shown in Table 4.2. Here the thickness seems to be decreasing with the increase in rpm for all samples which shows that the thickness is inversely related to the rpm. However, for the drop cast single layer ones, the thickness shows no consistency. For the thin films, the thickness is controlled by the spin coater whereas, in case of drop cast the thickness cannot be controlled.

Table 4.2: Thickness measurement of different samples averaged over 5 times

Thickness (mm)					
	Drop Cast	500 rpm	1000 rpm	2000 rpm	3000rpm
15-P-5	4.06±0.18	0.37±0.008	0.29±0.03	0.22±0.02	0.19±0.04
15-P-10	3.74±0.04	0.38±0.001	0.35±0.01	0.24±0.02	0.16±0.004
5-P-20	3.74±0.06	0.42±0.01	0.21±0.009	0.21±0.01	0.15±0.02
1%	2.13±0.01				
5%	2.24±0.01				
10%	2.66±0.007				
15%	2.10±0.01				
25%	2.84±0.004				

Chapter 5

Summary and Conclusion

All samples exhibit the pronounced, expected temperature dependence and are therefore useful for thermometry. Luminescence from the thinner samples is weaker but still worthwhile. Signals could readily be enhanced by using a brighter and focused source such as from a laser diode or other laser device. The thinnest samples were difficult to mount and test without tearing. More effort could be expended to arrange a mounting and fixturing approach to enable working with them in the future. Alternatively, there are formulations of PDMS that are more durable. They were not used in this study because of expense and availability.

The experiment with all the samples were done successfully. The luminescence results obtained from the samples in which phosphor powders are encapsulated within the elastomer is in well agreement with the results obtained from the powder only. So our aim of making a sensor from the powder embedded in the elastomer is achieved which also turn out to be flexible, detachable, reusable and an insulator. The temperature measured from two different amount of phosphor concentrated side were similar, thus they cannot be used as heat flux.

Summarizing, we can say that the sensor is made that can work in very cryogenic temperature as well as high temperature.

Chapter 6

Future Work

6.1 Use of different types of phosphor

Our aim with this experiment was to observe whether there will be a difference in luminescence from the thick and thin films. Also, if the amount of concentration of phosphor has an effect on the emissivity. However, the similarity in the emission obtained from all those samples gave us new ways of doing the experiment.

In the future, instead of using same phosphor on either side of the multiple layer, we can use two different phosphors on two different sides and observe the emission. It will be interesting to compare the luminescing properties obtained from these two samples. Also, in thin samples only, samples spun at 2000 rpm were taken for the study; thinner samples spun at 3000 rpm can be worked with in the future.

6.2 Preparing a patterned thermal sensor

Sensor that we have prepared measures the temperature of a large surface area. But when it comes to measure the temperature of something that is microns in size, then this sensor won't work properly as it will give us the information from a large area. Creating a pattern and preparing a sensor using the same pattern will be our next future work. This sensor when prepared will be useful in biology too as can measure the temperature of the cells. In

future, difficulty will be figuring out the way of pattern and creating that pattern itself.

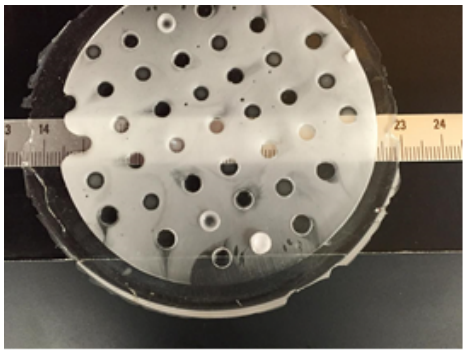

Figure 6.1: Pattern created in a neat Sylgard

Figure 6.1 is the one that we tried to create a pattern, however, the size of the holes turned out to be much bigger than our need. So, in future preparing similar kinds of sample with a hole size of microns will also be on our focus.

6.3 To observe the change in the measurement with the addition of carbon

All the carbon samples were prepared using 5% of carbon of the total amount and the characterization was done. In future, changes will be made regarding the concentration of the carbon powder and the changes in the different kinds of measurements will be studied.

6.4 Thermal expansion measurements

Observing the expansion of the samples by calculating their thermal expansion would be another focus of our work in the future since it will affect the thermal gradient across the sample.

Bibliography

[1] Sabri, F., Lynch, K. J., & Allison, S. (2015). Polymer-encapsulated phosphor particles for in vivo phosphor luminescence applications. *International Journal of Polymeric Materials and Polymeric Biomaterials*, 64(13), 690-694.

[2] Eldridge, J. I., Bencic, T. J., Allison, S. W., & Beshears, D. L. (2004). Depth-penetrating temperature measurements of thermal barrier coatings incorporating thermographic phosphors. *Journal of thermal spray technology*, 13(1), 44-50.

[3] Sabri, F., Sebelik, M. E., Meacham, R., Boughter Jr, J. D., Challis, M. J., & Leventis, N. (2013). In vivo ultrasonic detection of polyurea crosslinked silica aerogel implants. PloS one, 8(6), e66348.

[4] McKittrick, J., Shea, L. E., Bacalski, C. F., & Bosze, E. J. (1999). The influence of processing parameters on luminescent oxides produced by combustion synthesis. *Displays*, 19(4), 169-172.

[5] Pflitsch, C., Siddiqui, R. A., & Atakan, B. (2008). Phosphorescence properties of solgel derived ruby measured as functions of temperature and Cr3+ content. *Applied Physics A*, 90(3), 527-532.

[6] Tobin, K. W., Allison, S. W., Cates, M. R., Capps, G. J., & Beshears, D. L. (1990). High-temperature phosphor thermometry of rotating turbine blades. *AIAA journal*, 28(8), 1485-1490.

[7] Sabri, F., Lynch, K., Wilson, R., & Allison, S. W. (2014, June). Sensing with Phosphor-doped PDMS. *In Instrumentation Symposium 2014, IET & ISA 60th International* (pp. 1-6). IET.

[8] Eckbreth, A. C. (1996). *Laser diagnostics for combustion temperature and species (Vol. 3)*. CRC Press.

[9] McSherry, M., Fitzpatrick, C., & Lewis, E. (2005). Review of luminescent based fibre optic temperature sensors. *Sensor Review*, 25(1), 56-62.

[10] Mitchell, K. E., Gardner, V., Allison, S. W., & Sabri, F. (2016). Synthesis and characterization of flexible thermographic phosphor temperature sensors. *Optical Materials*, 60, 50-56.

[11] Sabri, F., Lynch, K. J., & Allison, S. (2015). Polymer-encapsulated phosphor particles for in vivo phosphor luminescence applications. International Journal of Polymeric Materials and Polymeric Biomaterials, 64(13), 690-694.

[12] Chen, D., Wan, Z., & Liu, S. (2016). Highly Sensitive Dual-Phase Nanoglass-Ceramics Self-Calibrated Optical Thermometer. *Analytical chemistry*, 88(7), 4099-4106.

[13] Fontenot, R. S., Allison, S. W., Lynch, K. J., Hollerman, W. A., & Sabri, F. (2016). Mechanical, spectral, and luminescence properties of ZnS: Mn doped PDMS. *Journal of Luminescence*, 170, 194-199.

[14] Allison, S. W., Baker, E. S., Lynch, K. J., & Sabri, F. (2015). In Vivo X-Ray Imaging of Phosphor-Doped PDMS and Phosphor-Doped Aerogel Biomaterials. International *Journal of Polymeric Materials and Polymeric Biomaterials*, 64(16), 823-830.

[15] Liu, M., Sun, J., Sun, Y., Bock, C., & Chen, Q. (2009). Thickness-dependent mechanical properties of polydimethylsiloxane membranes. Journal of micromechanics and microengineering, 19(3), 035028. Chicago

[16] Parks, J. E., Cates, M. R., Allison, S. W., Beshears, D. L., AlAkerman, M., & Scudiere, M. B. (2016). Temperature dependent fluorescence measurements. *Handbook of Measurement in Science and Engineering*, 3, 2225.

[17] Khalid, A. H., & Kontis, K. (2008). Thermographic phosphors for high temperature measurements: principles, current state of the art and recent applications. *Sensors*, 8(9), 5673-5744.

[18] Hansel, R. A. (2010), *Phosphor Thermometry Using Rare-Earth Doped Materials* (Proposal for Doctoral Dissertation). Retrieved from http://etd.library.vanderbilt.edu/available/etd-08052010-142925/unrestricted/thesis.pdf

[19] Parks, J. E. (2013). *Temperature Dependent Lifetime Measurements of Fluorescence from a Phosphor*, Presented at the 2013 AAPT Summer Meeting in Portland, Oregon.

[20] Tritt, T. M. (Ed.). (2005). Thermal conductivity: theory, properties, and applications. *Springer Science & Business Media*.

[21] Bouguerra, A., Ait-Mokhtar, A., Amiri, O., & Diop, M. B. (2001). Measurement of thermal conductivity, thermal diffusivity and heat capacity of highly porous building materials using transient plane source technique. *International communications in heat and mass transfer*, 28(8), 1065-1078.

[22] Janna, W. S. (2009) *Engineering Heat Transfer*, CRC Press.

[23] Al-Ajlan, S. A. (2006). Measurements of thermal properties of insulation materials by using transient plane source technique. *Applied thermal engineering*, 26(17), 2184-2191.

[24] ASTM, C. (1997). 177-85. Standard test method for steady-state heat flux measurements and thermal transmission properties by means of the guarded hot plate apparatus. *1992 annual book of ASTM standards*, 4, 20-31.

[25] ThermTest Inc. (2010), *TPS 1500 User's Manual*. Fredericton, NB, Canada.

[26] Han, Z., & Fina, A. (2011). Thermal conductivity of carbon nanotubes and their polymer nanocomposites: a review. *Progress in polymer science*, 36(7), 914-944.

[27] Liu, M., Sun, J., Sun, Y., Bock, C., & Chen, Q. (2009). Thickness-dependent mechanical properties of polydimethylsiloxane membranes. *Journal of micromechanics and microengineering*, 19(3), 035028.

[28] Johnston, I. D., McCluskey, D. K., Tan, C. K. L., & Tracey, M. C. (2014). Mechanical characterization of bulk Sylgard 184 for microfluidics and microengineering. *Journal of Micromechanics and Microengineering*, 24(3), 035017.

[29] Allison, S. W., Cates, M. R., Noel, B. W., & Gillies, G. T. (1988). Monitoring permanent-magnet motor heating with phosphor thermometry. *IEEE transactions on instrumentation and measurement*, 37(4), 637-641.

[30] Cates, M. R., Beshears, D. L., Allison, S. W., & Simmons, C. M. (1997). Phosphor thermometry at cryogenic temperatures. *Review of scientific instruments*, 68(6).

[31] Bianco, S., Pirri, C. F., Quaglio, M., Ferrario, P., & Castagna, R. (2011). *Nanocomposites based on elastomeric matrix filled with carbon nanotubes for biological applications*. INTECH Open Access Publisher.

[32] Sabri, F., Leventis, N., Hoskins, J., Schuerger, A. C., Sinden-Redding, M., Britt, D., & Duran, R. A. (2011). Spectroscopic evaluation of polyurea crosslinked aerogels, as a substitute for RTV-based chromatic calibration targets for spacecraft. *Advances in Space Research*, 47(3), 419-427.

[33] Sabri, F., Werhner, T., Hoskins, J., Schuerger, A. C., Hobbs, A. M., Barreto, J. A., & Duran, R. A. (2008). Thin film surface treatments for lowering dust adhesion on Mars Rover calibration targets. *Advances in Space Research*, 41(1), 118-128.

[34] Sabri, F., Marchetta, J., Faysal, K.R., Hewitt, R. and Roan, E., 2012. Mechanical Testing of Cross-linked Silica Aerogel Impregnated Silicone for Cryogenic Tank Applications. *In 50th AIAA Aerospace Sciences Meeting including the New Horizons Forum and Aerospace Exposition* (p. 1117).

[35] Fu, S. Y., Feng, X. Q., Lauke, B., & Mai, Y. W. (2008). Effects of particle size, particle/matrix interface adhesion and particle loading on mechanical properties of particulatepolymer composites. *Composites Part B: Engineering*, 39(6), 933-961.

[36] Sotebier, C., Michel, A., & Fresnais, J. (2012). Polydimethylsiloxane (PDMS) Coating onto Magnetic Nanoparticles Induced by Attractive Electrostatic Interaction. *Applied Sciences*, 2(2), 485-495.

[37] Sabri, F., Marchetta, J., & Smith, K. M. (2013). Thermal conductivity studies of a polyurea cross-linked silica aerogel-RTV 655 compound for cryogenic propellant tank applications in space. *Acta Astronautica*, 91, 173-179.